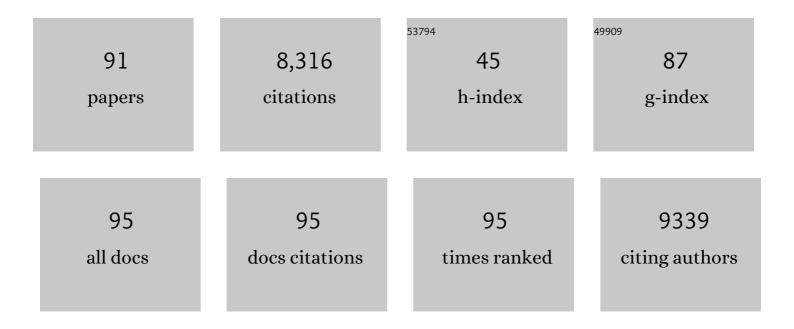
Jinguo Wang

List of Publications by Year in descending order

Source: https://exaly.com/author-pdf/11641978/publications.pdf Version: 2024-02-01



#	Article	IF	CITATIONS
1	Synthesis and Mechanistic Study of Palladium Nanobars and Nanorods. Journal of the American Chemical Society, 2007, 129, 3665-3675.	13.7	570
2	Synthesis and Characterization of 9 nm Pt–Ni Octahedra with a Record High Activity of 3.3 A/mg _{Pt} for the Oxygen Reduction Reaction. Nano Letters, 2013, 13, 3420-3425.	9.1	542
3	Atomic Layer-by-Layer Deposition of Pt on Pd Nanocubes for Catalysts with Enhanced Activity and Durability toward Oxygen Reduction. Nano Letters, 2014, 14, 3570-3576.	9.1	448
4	Synthesis of Pdâ^'Pt Bimetallic Nanocrystals with a Concave Structure through a Bromide-Induced Galvanic Replacement Reaction. Journal of the American Chemical Society, 2011, 133, 6078-6089.	13.7	405
5	Electrochemical Growth of Single-Crystal Metal Nanowires via a Two-Dimensional Nucleation and Growth Mechanism. Nano Letters, 2003, 3, 919-923.	9.1	362
6	On the role of surface diffusion in determining the shape or morphology of noble-metal nanocrystals. Proceedings of the National Academy of Sciences of the United States of America, 2013, 110, 6669-6673.	7.1	339
7	Synthesis of Pdâ [~] 'Au Bimetallic Nanocrystals via Controlled Overgrowth. Journal of the American Chemical Society, 2010, 132, 2506-2507.	13.7	252
8	Facile Synthesis of Pd–Pt Alloy Nanocages and Their Enhanced Performance for Preferential Oxidation of CO in Excess Hydrogen. ACS Nano, 2011, 5, 8212-8222.	14.6	236
9	Synthesis of Pdâ€Rh Core–Frame Concave Nanocubes and Their Conversion to Rh Cubic Nanoframes by Selective Etching of the Pd Cores. Angewandte Chemie - International Edition, 2012, 51, 10266-10270.	13.8	226
10	Facile Synthesis of Bimetallic Nanoplates Consisting of Pd Cores and Pt Shells through Seeded Epitaxial Growth. Nano Letters, 2008, 8, 2535-2540.	9.1	221
11	Atomic Layer-by-Layer Deposition of Platinum on Palladium Octahedra for Enhanced Catalysts toward the Oxygen Reduction Reaction. ACS Nano, 2015, 9, 2635-2647.	14.6	209
12	Synthesis of silver nanoplates at high yields by slowing down the polyol reduction of silver nitrate with polyacrylamide. Journal of Materials Chemistry, 2007, 17, 2600.	6.7	201
13	Template-Grown Metal Nanowires. Inorganic Chemistry, 2006, 45, 7555-7565.	4.0	194
14	Raman Scattering from Surface Phonons in Rectangular Cross-sectional w-ZnS Nanowires. Nano Letters, 2004, 4, 1991-1996.	9.1	190
15	Giant polarization in super-tetragonal thin films through interphase strain. Science, 2018, 361, 494-497.	12.6	173
16	Dissipation in quasi-one-dimensional superconducting single-crystalSnnanowires. Physical Review B, 2005, 71, .	3.2	172
17	Nanometer-Scale Modification and Welding of Silicon and Metallic Nanowires with a High-Intensity Electron Beam. Small, 2005, 1, 1221-1229.	10.0	171
18	Synthesis and Characterization of Pd@Pt–Ni Core–Shell Octahedra with High Activity toward Oxygen Reduction. ACS Nano, 2014, 8, 10363-10371.	14.6	165

#	Article	IF	CITATIONS
19	Copper Can Still Be Epitaxially Deposited on Palladium Nanocrystals To Generate Core–Shell Nanocubes Despite Their Large Lattice Mismatch. ACS Nano, 2012, 6, 2566-2573.	14.6	139
20	Facile Synthesis of Palladium Right Bipyramids and Their Use as Seeds for Overgrowth and as Catalysts for Formic Acid Oxidation. Journal of the American Chemical Society, 2013, 135, 15706-15709.	13.7	139
21	Microtwinning in Template-Synthesized Single-Crystal Metal Nanowires. Journal of Physical Chemistry B, 2004, 108, 841-845.	2.6	130
22	Penetrating the Oxide Barrier in Situ and Separating Freestanding Porous Anodic Alumina Films in One Step. Nano Letters, 2005, 5, 697-703.	9.1	128
23	Control Over the Branched Structures of Platinum Nanocrystals for Electrocatalytic Applications. ACS Nano, 2012, 6, 9797-9806.	14.6	126
24	Synthesis and characterization of superconducting single-crystal Sn nanowires. Applied Physics Letters, 2003, 83, 1620-1622.	3.3	120
25	Twinâ€Induced Growth of Palladium–Platinum Alloy Nanocrystals. Angewandte Chemie - International Edition, 2009, 48, 6304-6308.	13.8	119
26	Nanocrystals Composed of Alternating Shells of Pd and Pt Can Be Obtained by Sequentially Adding Different Precursors. Journal of the American Chemical Society, 2011, 133, 10422-10425.	13.7	115
27	Continuous and Scalable Production of Well-Controlled Noble-Metal Nanocrystals in Milliliter-Sized Droplet Reactors. Nano Letters, 2014, 14, 6626-6631.	9.1	113
28	Effect of Ti interlayer on interfacial thermal conductance between CuÂand diamond. Acta Materialia, 2018, 160, 235-246.	7.9	111
29	Pt–Ni octahedral nanocrystals as a class of highly active electrocatalysts toward the hydrogen evolution reaction in an alkaline electrolyte. Journal of Materials Chemistry A, 2016, 4, 12392-12397.	10.3	103
30	Suppression of Superconductivity in Zinc Nanowires by Bulk Superconductors. Physical Review Letters, 2005, 95, 076802.	7.8	96
31	<i>In Situ</i> TEM Characterization of Shear-Stress-Induced Interlayer Sliding in the Cross Section View of Molybdenum Disulfide. ACS Nano, 2015, 9, 1543-1551.	14.6	93
32	Synthesis of Pt–Ni Octahedra in Continuous-Flow Droplet Reactors for the Scalable Production of Highly Active Catalysts toward Oxygen Reduction. Nano Letters, 2016, 16, 3850-3857.	9.1	86
33	Optimized thermal properties in diamond particles reinforced copper-titanium matrix composites produced by gas pressure infiltration. Composites Part A: Applied Science and Manufacturing, 2016, 91, 189-194.	7.6	80
34	Enhanced thermal conductivity in Cu/diamond composites by tailoring the thickness of interfacial TiC layer. Composites Part A: Applied Science and Manufacturing, 2018, 113, 76-82.	7.6	80
35	Observation of Superconductivity in Granular Bi Nanowires Fabricated by Electrodeposition. Nano Letters, 2006, 6, 2773-2780.	9.1	79
36	Combining Cr pre-coating and Cr alloying to improve the thermal conductivity of diamond particles reinforced Cu matrix composites. Journal of Alloys and Compounds, 2018, 749, 1098-1105.	5.5	78

#	Article	lF	CITATIONS
37	Photochemical Deposition of Highly Dispersed Pt Nanoparticles on Porous CeO ₂ Nanofibers for the Waterâ€Gas Shift Reaction. Advanced Functional Materials, 2015, 25, 4153-4162.	14.9	75
38	High thermal conductivity of Cu-B/diamond composites prepared by gas pressure infiltration. Journal of Alloys and Compounds, 2018, 735, 1648-1653.	5.5	75
39	Confining the Nucleation and Overgrowth of Rh to the {111} Facets of Pd Nanocrystal Seeds: The Roles of Capping Agent and Surface Diffusion. Journal of the American Chemical Society, 2013, 135, 16658-16667.	13.7	73
40	Controlling the Size and Composition of Nanosized Pt–Ni Octahedra to Optimize Their Catalytic Activities toward the Oxygen Reduction Reaction. ChemSusChem, 2014, 7, 1476-1483.	6.8	72
41	Synthesis of Rhodium Concave Tetrahedrons by Collectively Manipulating the Reduction Kinetics, Facet-Selective Capping, and Surface Diffusion. Nano Letters, 2013, 13, 6262-6268.	9.1	66
42	Tailoring interface structure and enhancing thermal conductivity of Cu/diamond composites by alloying boron to the Cu matrix. Materials Characterization, 2019, 152, 265-275.	4.4	66
43	Interfacial structure evolution of Ti-coated diamond particle reinforced Al matrix composite produced by gas pressure infiltration. Composites Part B: Engineering, 2017, 113, 285-290.	12.0	56
44	Interfacial structure evolution and thermal conductivity of Cu-Zr/diamond composites prepared by gas pressure infiltration. Journal of Alloys and Compounds, 2019, 781, 800-809.	5.5	50
45	Nucleation and growth mechanisms of interfacial Al 4 C 3 in Al/diamond composites. Journal of Alloys and Compounds, 2016, 657, 81-89.	5.5	46
46	Facile synthesis of Pd–Ir bimetallic octapods and nanocages through galvanic replacement and co-reduction, and their use for hydrazine decomposition. Physical Chemistry Chemical Physics, 2013, 15, 11822.	2.8	42
47	Regulated Interfacial Thermal Conductance between Cu and Diamond by a TiC Interlayer for Thermal Management Applications. ACS Applied Materials & Interfaces, 2019, 11, 26507-26517.	8.0	41
48	Atomic and electronic structure of Lomer dislocations at CdTe bicrystal interface. Scientific Reports, 2016, 6, 27009.	3.3	35
49	Enhanced shape stability of Pd–Rh core–frame nanocubes at elevated temperature: in situ heating transmission electron microscopy. Chemical Communications, 2013, 49, 11806.	4.1	33
50	Strong Second Harmonic Generation in a Tungsten Bronze Oxide by Enhancing Local Structural Distortion. Journal of the American Chemical Society, 2020, 142, 7480-7486.	13.7	33
51	The role of Cr interlayer in determining interfacial thermal conductance between Cu and diamond. Applied Surface Science, 2020, 515, 146046.	6.1	32
52	Influence of a bulk superconducting environment on the superconductivity of one-dimensional zinc nanowires. Physical Review B, 2006, 74, .	3.2	30
53	Seed-mediated synthesis of Pd–Rh bimetallic nanodendrites. Chemical Physics Letters, 2010, 494, 249-254.	2.6	30
54	The formation of atomic-level interfacial layer and its effect on thermal conductivity of W-coated diamond particles reinforced Al matrix composites. Composites Part A: Applied Science and Manufacturing, 2018, 107, 164-170.	7.6	29

#	Article	IF	CITATIONS
55	A Mechanistic Study on the Nucleation and Growth of Au on Pd Seeds with a Cubic or Octahedral Shape. ChemCatChem, 2012, 4, 1668-1674.	3.7	28
56	Interfacial products and thermal conductivity of diamond/Al composites reinforced with ZrC-coated diamond particles. Diamond and Related Materials, 2019, 100, 107565.	3.9	28
57	Aberration Corrected Electron Microscopy Study of Bimetallic Pd–Pt Nanocrystal: Core–Shell Cubic and Core–Frame Concave Structures. Journal of Physical Chemistry C, 2014, 118, 28876-28882.	3.1	26
58	Effect of diamond surface chemistry and structure on the interfacial microstructure and properties of Al/diamond composites. RSC Advances, 2016, 6, 67252-67259.	3.6	24
59	Proton-Conducting Films of Nanoscale Ribbons Formed by Exfoliation of the Layer Perovskite H2SrTa2O7. Chemistry of Materials, 2008, 20, 213-219.	6.7	21
60	Creating a single twin boundary between two CdTe (111) wafers with controlled rotation angle by wafer bonding. Applied Physics Letters, 2013, 103, .	3.3	21
61	Effects of metal gate-induced strain on the performance of metal-oxide-semiconductor field effect transistors with titanium nitride gate electrode and hafnium oxide dielectric. Applied Physics Letters, 2007, 91, .	3.3	18
62	Mo-interlayer-mediated thermal conductance at Cu/diamond interface measured by time-domain thermoreflectance. Composites Part A: Applied Science and Manufacturing, 2020, 135, 105921.	7.6	17
63	Unveiling interfacial structure and improving thermal conductivity of Cu/diamond composites reinforced with Zr-coated diamond particles. Vacuum, 2022, 202, 111133.	3.5	17
64	Tunable coefficient of thermal expansion of Cu-B/diamond composites prepared by gas pressure infiltration. Journal of Alloys and Compounds, 2019, 794, 473-481.	5.5	16
65	Aluminum carbide hydrolysis induced degradation of thermal conductivity and tensile strength in diamond/aluminum composite. Journal of Composite Materials, 2018, 52, 2709-2717.	2.4	14
66	One-step <i>in situ</i> growth of ZnS nanoparticles on reduced graphene oxides and their improved lithium storage performance using sodium carboxymethyl cellulose binder. RSC Advances, 2018, 8, 9125-9133.	3.6	13
67	Effects of Al substitution on the spontaneous polarization and lattice dynamics of the PbTi1â^'xAlxO3. Dalton Transactions, 2010, 39, 5183.	3.3	12
68	Compression Properties and Electrical Conductivity of In-Situ 20 vol.% Nano-Sized TiCx/Cu Composites with Different Particle Size and Morphology. Materials, 2017, 10, 499.	2.9	12
69	Controllable Ferromagnetism in Super-tetragonal PbTiO ₃ through Strain Engineering. Nano Letters, 2020, 20, 881-886.	9.1	11
70	Grain Refinement and Mechanical Properties of Cu–Cr–Zr Alloys with Different Nano-Sized TiCp Addition. Materials, 2017, 10, 919.	2.9	10
71	Detection of nucleotides in hydrated ssDNA via 2D hâ€BN nanopore with ionicâ€liquid/salt–water interface. Electrophoresis, 2021, 42, 991-1002.	2.4	10
72	Shape-Controlled TiCx Particles Fabricated by Combustion Synthesis in the Cu-Ti-C System. Crystals, 2017, 7, 205.	2.2	9

#	Article	IF	CITATIONS
73	Aqueous Synthesis of Pd–M (M = Pd, Pt, and Au) Decahedra with Concave Facets for Catalytic Applications. Topics in Catalysis, 2020, 63, 664-672.	2.8	9
74	Hydrogenated amorphous silicon nanowire transistors with Schottky barrier source/drain junctions. Applied Physics Letters, 2010, 97, .	3.3	8
75	Luminescent LaF3:Ce-doped organically modified nanoporous silica xerogels. Journal of Applied Physics, 2013, 113, .	2.5	8
76	Site-selective sulfurization of bromide-capped palladium nanocubes by polysulfide and the underlying mechanism. Nanotechnology, 2014, 25, 014003.	2.6	8
77	Effect of Cu-Ti-C reaction composition on reinforcing particles size of TiC x /Cu composites. Journal Wuhan University of Technology, Materials Science Edition, 2018, 33, 43-48.	1.0	8
78	Microstructural evolution of sandwiched Cr interlayer in Cu/Cr/diamond subjected to heat treatment. Thin Solid Films, 2021, 736, 138911.	1.8	8
79	Microstructure and Enhanced Properties of Copper-Vanadium Nanocomposites Obtained by Powder Metallurgy. Materials, 2019, 12, 339.	2.9	6
80	Study on electroless Cu plating quality of in situ TiCp. Scientific Reports, 2020, 10, 12196.	3.3	4
81	Atomic Resolution Scanning Transmission Electron Microscopy of Two-Dimensional Layered Transition Metal Dichalcogenides. Applied Microscopy, 2015, 45, 225-229.	1.4	4
82	Creating Single Boundary between Two CdTe (111) Wafers with Controlled Orientation by Wafer Bonding. Microscopy and Microanalysis, 2014, 20, 516-517.	0.4	1
83	Aberration Corrected High Angle Annular Dark Field (HAADF) Scanning Transmission Electron Microscopy (STEM) and In Situ Transmission Electron Microscopy (TEM) Study of Transition Metal Dichalcogenides (TMDs). Microscopy and Microanalysis, 2015, 21, 431-432.	0.4	1
84	Simple Specimen Preparation Method for In Situ Heating Experiments. Microscopy and Microanalysis, 2016, 22, 132-133.	0.4	1
85	A Method to Prepare TEM Specimens by Focused Ion Beam Milling for Cu/diamond Composites. Microscopy and Microanalysis, 2018, 24, 838-839.	0.4	1
86	Microstructure and Superconductivity of Zn and Au-Sn Junction Nanowires. Journal of Nanoscience and Nanotechnology, 2009, 9, 946-950.	0.9	0
87	In-Situ Studies of Thermal Stability of Core–Frame Cubic Pd–Rh Nanocrystals at Elevated Temperatures. Microscopy and Microanalysis, 2014, 20, 1632-1633.	0.4	0
88	Aberration-Corrected STEM and Tomography of Pd-Pt Nanoparticles: Core-Shell Cubic and Core-Frame Concave Structures. Microscopy and Microanalysis, 2015, 21, 1731-1732.	0.4	0
89	Aberration-Corrected STEM Study of Shape Controlled Metallic Core-Shell Nanoparticles for Catalytic Applications. Microscopy and Microanalysis, 2017, 23, 1852-1853.	0.4	0
90	Probing Nanoscale Local Lattice Strains in Semiconductor Nanostructures and Devices by Transmission Electron Microscopy. Microscopy and Microanalysis, 2018, 24, 972-973.	0.4	0

#	Article	IF	CITATIONS
91	Interface tailoring and thermal conductivity enhancement in diamond particles reinforced metal matrix composites. , 2020, , 473-493.		0